Materials Advances

ROYAL SOCIETY OF CHEMISTRY

PAPER

View Article Online
View Journal | View Issue

Cite this: *Mater. Adv.*, 2026, 7, 509

Tailored magnetic hybrid composites with recoverable properties for efficient Cr(VI) adsorption and reduction: a synergistic experimental and theoretical study

Abdelaziz Imgharn, *[ab] Mohammed Elhoudi,[a] Samira El omari,[a] Kamal Ait El Bacha,[a] Mohamed Laabd,[a] Lahcen Bazzi[c] and Abdallah Albourine[ac]

Despite polyaniline's simple synthesis methods and proven capabilities pollutant removal applications, its recovery from solutions remains a major challenge that hampers its application. Therefore, developing approaches for synthesizing an efficient and easily recoverable polyaniline (PANI) adsorbent is crucial. In this study, we designed a magnetic Fe_3O_4–cysteine-functionalized PANI (Fe_3O_4–Cys–PANI) adsorbent *via in situ* polymerization. The resulting magnetic adsorbent was characterized by several analytical techniques (*e.g.*, FTIR spectroscopy, XRD, porosity measurements and SEM-EDS), and the results indicated that it exhibited tunable features for Cr(VI) detoxification. A systematic experimental study revealed that the maximum Cr(VI) detoxification yield (98.12%) was achieved with an adsorbent dose of 0.25 g L^{-1} and at pH 2.0. The Freundlich isotherm models and the pseudo-second-order kinetics were appropriate for predicting the Cr(VI) removal process. The Monte Carlo simulations further elucidated the Cr(VI) adsorption process, revealing an adsorption energy of E_{ads} = −55.613 kcal mol^{-1} on Fe_3O_4–Cys–PANI. The significantly negative adsorption energy further supported the experimental findings, confirming the spontaneity of the process and high energy efficiency. Additionally, the Fe_3O_4–Cys–PANI magnetic composite showed excellent decontamination, outstanding regeneration capacity and prominent reusability, making it a promising candidate for industrial wastewater treatment.

Received 16th August 2025,
Accepted 26th October 2025

DOI: 10.1039/d5ma00917k

rsc.li/materials-advances

1. Introduction

Chromium (Cr) toxins are found in almost every component of the environment, including soil, air, and water.[1–3] Cr(VI) oxyanions, common forms of the heavy metal chromium, raise a significant concern due to their toxic properties and tendency to accumulate in organisms. Acute exposure to Cr(VI) can lead to diarrhea, kidney failure, nausea, liver diseases, ulcer formation, lung cancer and respiratory issues.[4,5] Reducing Cr(VI) to Cr(III) is indeed an ideal option, given the much higher toxicity of Cr(VI) compared to Cr(III).[6] Hence, it is crucial to explore and develop effective methods that can concurrently reduce Cr(VI) to Cr(III) and eliminate it from the environment. The conventional approaches for wastewater treatment involve membrane filtration, electrochemical processes, coagulation and flocculation, bioremediation, and advanced oxidation processes.[4,6] Nevertheless, these approaches require high-energy systems, which can increase their operating costs. It is particularly advantageous to adsorb and reduce Cr(VI) ions from solutions using the adsorption–reduction process. Thus, it is essential to develop low-cost, dual-purpose, and highly efficient materials for adsorption–reduction.

A variety of N-containing functional group organic polymers have been used in hybrid composites in recent years to adsorb and reduce Cr(VI).[7–9] The unique conjugation system, doping/dedoping properties, and excellent stability of these composites have led to their excessive use in hybrids. Besides their interrelationship with Cr(VI)'s negative charge, nitrogen atoms in amines and imines can donate electrons to reduce Cr(VI) ions into less-toxic Cr(III) ions.[10] Therefore, polyaniline (PANI) possesses all the aforementioned features, making it a promising adsorber/reducer for Cr(VI) detoxification.[11] Recent investigations have reaffirmed its outstanding performance in Cr(VI) removal and revealed its potential for the adsorption of a wide range of organic pollutants from aqueous media. Nevertheless, as for other adsorbent materials, the main cornerstone of PANI for further application in the field of adsorption is its difficult

[a] *Laboratory of Materials and Environment, Faculty of Sciences, Ibn Zohr University, Agadir, Morocco. E-mail: abdelaziz.imgharn@edu.uiz.ac.ma*
[b] *International Water Research Institute (IWRI), Mohammed VI Polytechnic University, Ben Guerir 43150, Morocco*
[c] *Laboratory of Industrial Engineering, Energy and Environment (LI3E), SupMTI Rabat, Morocco*

recovery from solutions, which can lead to secondary pollution. Due to the absence of polarity on PANI, it cannot be controlled by magnetic fields.[12] Typically, PANI powders are separated from liquid solutions by centrifugation or filtration, both of which are expensive.[13,14]

To address this issue and prevent secondary pollution after adsorption processes, incorporating magnetic materials enables easy recovery. It is therefore proposed to combine PANI with magnetic particles to adsorb heavy metals in a simple, low-cost and fast way for practical procedures.[15–17] The Fe_3O_4 magnetic particles were chosen not only to tackle the PANI's drawback – its recovery – but also to contribute toward the reduction of toxic Cr(VI) to the less harmful Cr(III) form, making it an efficient water purification material.[10,18] Furthermore, functionalizing PANI with cysteine significantly enhances its adsorption capacity and selectivity for Cr(VI) by introducing additional functional groups that facilitate strong and selective binding of Cr(VI) oxyanions. Magnetic cysteine–PANI composites have not yet been reported, representing an efficient approach that combines enhanced adsorption performance with the magnetic functionality that ensures easy recovery and reusability of the adsorbent. This integration ensures efficient pollutant removal and prevents secondary contamination of water by facilitating its separation from treated water.

This research endeavor holds immense significance in the field of water environmental remediation, aiming to mitigate the detrimental effects of Cr(VI) in water systems. Herein, a tailored hybrid composite was developed and characterized, in which Fe_3O_4, cysteine and polyaniline were combined to provide functional groups, magnetic recoverability, and improved Cr(VI) adsorption capacity. A systematic study was conducted to evaluate the influences of solution pH, temperature, adsorbent dose, contact time and selectivity on the Cr(VI) detoxification. Finally, the regeneration of Fe_3O_4–Cys–PANI was performed to assess its reusability.

2. Experimental

2.1. Chemicals

Aniline (C_6H_7N) (≥99%), sodium hydroxide (NaOH) (≥99%), ammonium persulfate ($(NH_4)_2S_2O_8$) (≥98.5%), ammonia (NH_4OH) (≥99%), iron(III) chloride ($FeCl_3{\cdot}6H_2O$) (≥99%), iron(II) chloride ($FeCl_2{\cdot}4H_2O$) (≥98.8%), ethanol (C_2H_6O) (≥99%), acetone (≥99.8%), hydrochloric acid (HCl) (37%), potassium dichromate ($K_2Cr_2O_7$) (≥99.5%), phosphoric acid (H_3PO_4) (86%), 1,5-diphenylcarbazide (95%) and sulfuric acid (H_2SO_4) (≥98%) were purchased from Sigma-Aldrich.

2.2. Preparation of magnetic Fe_3O_4–Cys–PANI with recoverability

The Fe_3O_4 nanoparticles were synthesized by a co-precipitation method. Briefly, 1 M $FeCl_2{\cdot}4H_2O$ and 2 M $FeCl_3{\cdot}6H_2O$ were introduced into deionized water at a molar ratio of 1/2. NH_4OH (2 M) was added dropwise to the solution under continuous stirring at 60 °C for 4 h. The resulting nanoparticles were magnetically separated, washed with distilled water, and dried at 70 °C.

The magnetic Fe_3O_4–Cys–PANI composite was synthesized *via in situ* oxidative polymerization in an ice bath. In this process, 1 g of Fe_3O_4 nanoparticles and 1 g of cysteine were first dispersed in 100 mL of 0.01 M HCl and sonicated for 1 h to ensure uniform distribution and surface functionalization. Subsequently, 0.25 mL of purified aniline monomer was introduced into the Fe_3O_4–cysteine suspension, allowing cysteine to act as a co-functional agent during the polymerization step. The mixture was then stirred for 2 h. Then, ammonium persulfate (APS), dissolved in 50 mL of 0.01 M HCl with a 1/2 monomer (aniline)-to-oxidant (APS) molar ratio, was added dropwise to the suspension while maintaining the ice bath. Polymerization proceeded under continuous stirring for 12 h. The resulting Fe_3O_4–Cys–PANI composite was washed with ethanol and distilled water and dried at 70 °C. This tailored design strategy was selected to combine the high affinity of cysteine functional groups, the conductive framework of PANI, and the magnetic separability of Fe_3O_4, thereby enhancing the overall adsorption efficiency.

2.3. Characterization of the adsorbent

The porosity of Fe_3O_4–Cys–PANI was evaluated by N_2 adsorption at −196 °C in a volumetric analyzer. Prior to the measurements, the sample was outgassed at 120 °C for 12 h under vacuum. The total pore volume (V_{total}), specific surface area (S_{BET}), and the micropore volume (V_{MICRO}) were acquired from the gas adsorption data. The Fe_3O_4–Cys–PANI surface features were visualized by scanning electron microscopy (SEM, JEOL JSM-IT200, operating at an accelerating voltage of 10–20 kV) coupled with energy-dispersive X-ray spectrometry (EDS) analysis. The zero-charge point (PZC) of the Fe_3O_4–Cys–PANI sample was investigated by a potentiometric titration route. The crystal structures of the hybrid composites were investigated by X-ray powder diffraction (XRD) analysis (EMPYREAN PANALYTICAL diffractometer). Fourier-transform infrared (FTIR) spectra of the prepared materials were visualized using an FT-IR spectrometer (ALPHA-Bruker Optics, Germany) with KBr pellets in the range of 400 to 4000 cm^{-1}.

2.4. Batch experiments and regeneration

The adsorption assays were conducted to evaluate Cr(VI) decontamination on the Fe_3O_4–Cys–PANI surface. The tests were carried out in Erlenmeyer flasks containing 20 mg L^{-1} Cr(VI) solutions (100 mL) with the composite studied (0.025 g) under continuous stirring at constant temperature. After each adsorption experiment, Fe_3O_4–Cys–PANI was separated easily from the Cr(VI) solution by a magnet. The equilibrium concentration of Cr(VI) was complexed with 1,5-diphenylcarbazide and then analyzed using a UV-2300 spectrophotometer at 540 nm. The removed efficiency R(%) and the adsorption uptake Q_e (mg g^{-1}) were determined using the following equations:[19]

$$R\% = \frac{(C_0 - C_e)}{C_0} \times 100 \quad (1)$$

$$Q_e = \frac{(C_0 - C_e) \cdot V}{m} \quad (2)$$

where C_0 (mg L^{-1}) is the initial Cr(VI) concentration, C_e (mg L^{-1}) is the Cr(VI) concentration at equilibrium, and m (g) is the amount of the Fe_3O_4–Cys–PANI composite.

Water treatment involves regenerating adsorbents to restore their original properties for reuse.[20] In this process, after recovering the material using a magnet after its use, 50 mL of 0.4 M NaOH solution was added to an Erlenmeyer flask containing Fe_3O_4–Cys–PANI and soaked for 2 hours at 25 °C. After soaking in NaOH, the regenerated sample was rinsed with distilled water and then treated with 0.8 M HCl. Subsequently, a fresh Cr(VI) solution was used under the same conditions for five adsorption–desorption runs.

2.5. Computational details

2.5.1. DFT calculation details. The molecular structures of polyaniline (PANI) and cysteine were constructed using the GaussView software.[21] Geometry optimization of the cysteine-functionalized polyaniline was performed using the Perdew–Burke–Ernzerhof (PBE) functional within the generalized gradient approximation (GGA) for the exchange–correlation energy.[22] For systems involving metal atoms, the LANL2DZ (Los Alamos National Laboratory 2 double-zeta) basis set was employed, incorporating effective core potential (ECP) functions to reduce the computational cost.[23] It has been demonstrated that the functional provides reliable geometries for a wide range of systems.[24–26] All calculations were carried out using the 6-311++g(d,p) basis set within the Gaussian 09 package.[27] The computations were performed in an aqueous solution using the polarized continuum model (PCM) of solvation based on the integral equation formalism.[28] To confirm that the optimized structure corresponded to a true minimum on the potential energy surface, a harmonic frequency calculation was performed at the same theoretical level.[29,30]

2.5.2. Monte Carlo/SA simulation details. To gain deeper insights into the adsorption process of Cr(VI) ions on the Fe_3O_4–cysteine-functionalized–polyaniline (Fe_3O_4–Cys–PANI) hybrid composite in aqueous systems, the Metropolis Monte Carlo simulations combined with the simulated annealing (SA) algorithm were performed.[31,32] To closely reproduce the real system, the Monte Carlo/SA simulations were conducted by explicitly including the solvent effect, using $50H_2O + 1H_3O^+ +$ 1Cr(VI) solution's composition. The simulations were performed using three heating ramps, with 3×10^4 Monte Carlo steps per ramp. The candidate adsorbate–substrate configurations were sampled from a canonical ensemble, in which the number of adsorbate molecules, substrate loading, and temperature were kept constant. The resulting adsorbate–substrate system was pre-geometrized using the DFT at the PBE-6-311++g(d,p) level of theory to ensure the realistic initial geometry. In the present investigation, the convergence tolerances for energy, force, and displacement were fixed at 10^{-4} kcal mol^{-1}, 0.005 kcal mol^{-1} $Å^{-1}$ and 3×10^{-5} Å, respectively. Electrostatic and van der Waals forces were computed using Ewald and atom-based summation methods, respectively. In order to optimize the structure of all components of the systems, the CVFF force field was used.

The crystallographic structure of studied Fe_3O_4 was obtained from previous studies.[33,34] To predict the more adapted Fe_3O_4 surfaces for the simulations process, DFT with a plane-wave basis set was utilized. As a result, the simulations were carried out on Fe_3O_4 periodic crystal surfaces in a simulation box of 30.16 Å × 30.16 Å × 23.29 Å, which consists of 15 Å of substrates and a vacuum region of 30 Å thickness. The adsorption (E_{Ads}) energy of Cr(VI) ions on each substrate type was calculated using eqn (3):[35]

$$E_{ads} = E_{syst} - (E_{subs/surf+sol} + E_{iso/subs}) \quad (3)$$

where E_{syst} is the total energy of the studied system, $E_{subs/surf+sol}$ denotes the energy of the substrate surface solution interface, $E_{iso/subs}$ presents the energy of the free substrate, respectively.

All computations were performed using the BIOVIA Materials Studio 6.0 software package (Dassault Systèmes, San Diego).[36]

3. Results and discussion

3.1. Characterization

3.1.1. Morphology and porosity. The SEM analysis was conducted to investigate the morphological characteristics of both the Fe_3O_4 and Fe_3O_4–Cys–PANI surfaces. Fe_3O_4 (Fig. 1(a)) showed the agglomeration of irregularly shaped particles, attributed to their magnetic characteristics. As shown in Fig. 1(b), the formation of Cys–PANI on Fe_3O_4 particles resulted in a significant change in the morphology of the sample. This change affirms the core–shell surface of the Fe_3O_4–Cys–PANI magnetic composite. The EDS analysis identified the elements present on the Fe_3O_4 and Fe_3O_4–Cys–PANI surfaces, as shown in Fig. 1(c) and (d), respectively. The Fe_3O_4 surface (Fig. 1(c)) exhibited the presence of O and Fe elements. Fig. 1(d) illustrates the occurrence of these elements along with C, N, S and Cl, indicating the formation of the Fe_3O_4–Cys–PANI magnetic composite.

The specific surface area of Fe_3O_4–Cys–PANI was determined using isothermal N_2 adsorption–desorption measurements, as shown in Fig. 1(e). In conformity with the IUPAC classification, the N_2 adsorption–desorption isotherm of our adsorbent shows a typical IV isotherm with a H3-type hysteresis loop, thus indicating the occurrence of mesoporous structures (with pore sizes between 2 and 50).[37] Furthermore, its surface area composite is about 19 m^2 g^{-1} and the total pore volume is 0.046 cm^3 g^{-1}.

3.1.2. FTIR spectroscopy and XRD analyses. The FTIR spectrum of Fe_3O_4 displays the distinctive peaks of the Fe–O bond at 550 and 1645 cm^{-1}, providing evidence for the formation of pure Fe_3O_4 (Fig. 2(a)).[38] The FTIR spectrum of Fe_3O_4–Cys–PANI provides the presence of a band at 3351 cm^{-1}, which is ascribed to the N–H stretching vibrations.[39,40] This band overlaps with a similar band accredited to the $-NH_3^+$ stretching

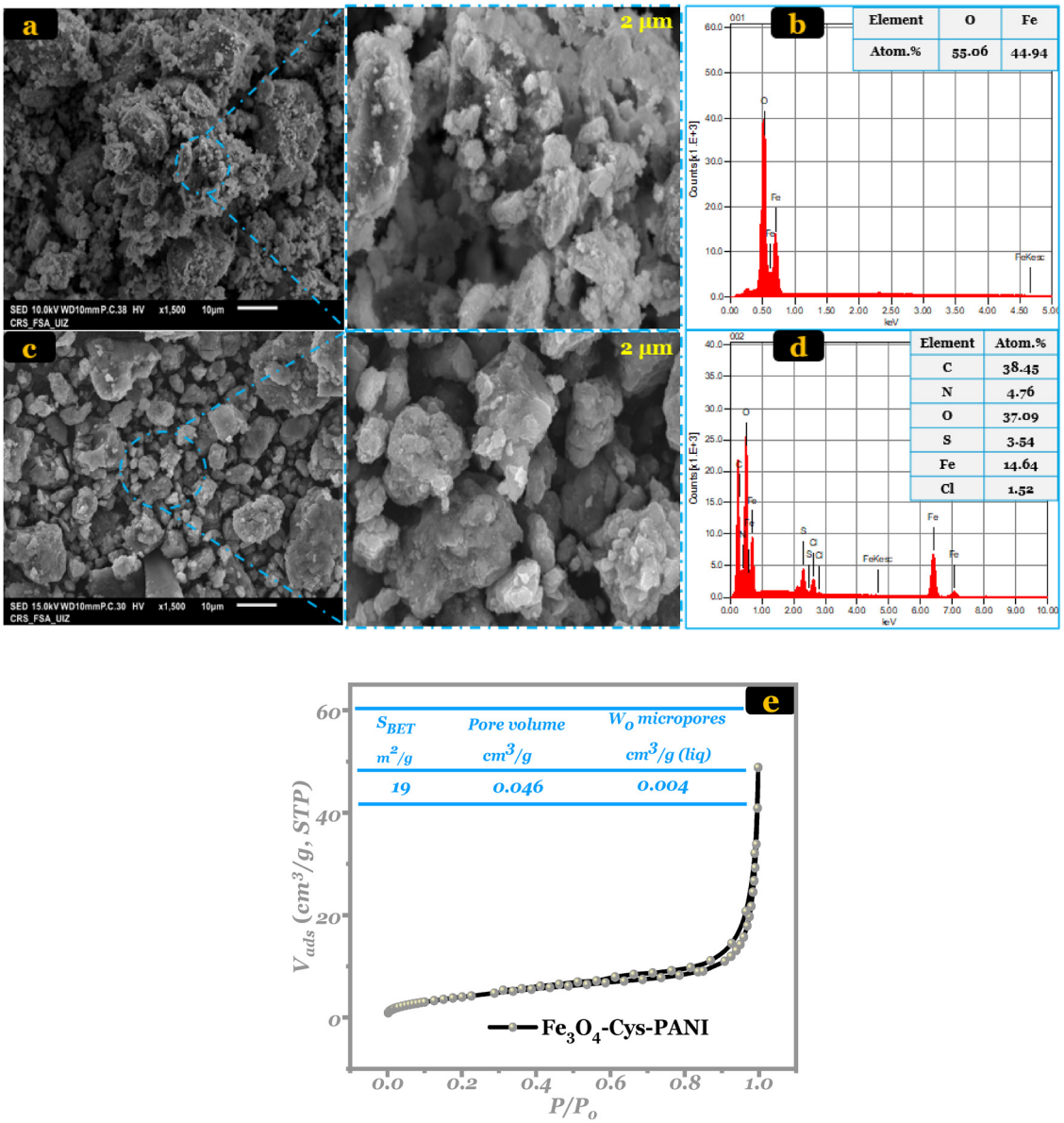

Fig. 1 (a) SEM images of Fe_3O_4 and (c) Fe_3O_4–Cys–PANI and their corresponding (b) and (d) EDS elemental spectra. (e) N_2 adsorption isotherms curves of Fe_3O_4–Cys–PANI.

vibrations, which correspond to cysteine. In addition to this overlapped band located at 3045 cm^{-1}, two bands are noticed at 1590 and 1395 cm^{-1}, which are attributed to the symmetric and asymmetric stretching vibrations of the carboxylate group ($-COO^-$), respectively. Moreover, a distinct band appearing at around 1500 cm^{-1} is assigned to the C=N stretching vibration of the quinoid structure in PANI, confirming its successful polymerization.[41,42] A weak peak at 2575 cm^{-1} corresponds to the S–H stretching vibrations.[10] Furthermore, all other characteristic absorption bands of Fe_3O_4 are observed in the spectra of Fe_3O_4–Cys–PANI composite. It is noteworthy that there is a decrease in the intensity of the peak at 580 cm^{-1}, attributed to Fe_3O_4, accompanied by a slight shift observed in the band at 550 cm^{-1}, which moves to 558 cm^{-1}. This shift indicates the interaction between Fe_3O_4 and Cys–PANI in the composite.

The XRD patterns of cysteine and Fe_3O_4–Cys–PANI are presented in Fig. 2(b). The XRD analyses were performed to examine the phase and crystal structure of the synthesized materials. The findings indicate that the XRD pattern of pure Fe_3O_4 corresponds to orthorhombic magnetite (JCPDS 75-1609, space group Imma and no. 74).[43] Notably, the diffraction peaks observed at 2θ = 18.49, 30.34°, 35.65°, 43.31°, 53.82°, 57.32°, and 62.93° can be ascribed to the crystal planes of (0 1 1), (2 0 0), (1 0 3), (0 0 4), (2 0 4), (3 2 1), and (4 0 0), respectively. For cysteine, the pattern shows main peaks centered at 18.91° (1 0 0), 28.58° (0 0 1), 33.12° (1 1 2), 34.45° (1 1 6) and 38.44° (2 0 3), according to JCPDS 37-1802.[44] The Fe_3O_4–Cys–PANI diffractogram depicts the coexistence of both Fe_3O_4 and cysteine phases with a reduction in the intensity of their main peaks. Additionally, the lack of impurity in the XRD patterns

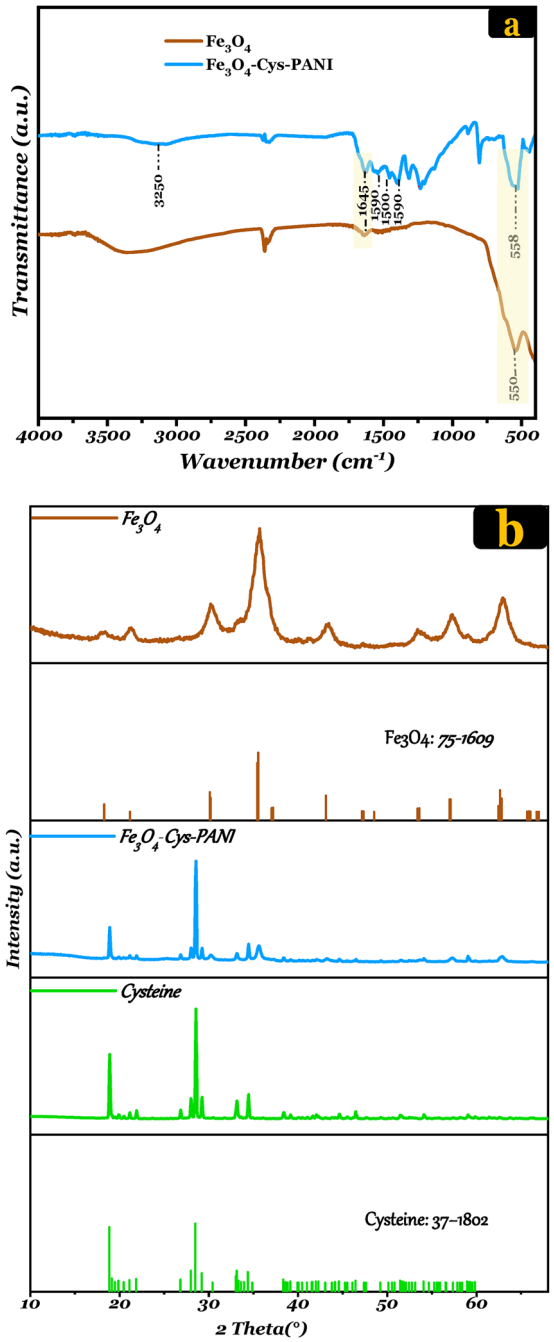

Fig. 2 (a) XRD patterns of Fe_3O_4 and Fe_3O_4–Cys–PANI composite. (b) FTIR spectra of Fe_3O_4, Cysteine and Fe_3O_4–Cys–PANI.

suggests the successful design of the Fe_3O_4–Cys–PANI composite. In addition, the crystallite size was calculated using the Scherrer equation (eqn (4)):

$$D = \frac{K\lambda}{\beta \cos\theta} \quad (4)$$

where form factor K tunes from 0.62 to 2.08, depending on the morphology,[45] the wavelength of the X-ray radiation is denoted by λ, β is the full width at half maximum (FWHM) in radians of the peak and θ is the diffraction angle in radians.[46,47] The prepared magnetic composite has a relatively small nanostructure with a crystallite size of 49 nm, but its moderate surface area of 19 $m^2\ g^{-1}$ suggests that Cr(VI) decontamination efficiency is likely influenced more by its chemical properties than its surface area alone, as will be discussed below.

3.2. Adsorption experiments

3.2.1. Loading, pH effects and mechanism

Loading effect. The impact of loading on the detoxification of 20 ppm Cr(VI) was investigated in the 0.125–1.5 g L^{-1} loading range. It can be observed from Fig. 3(a) that the Cr(VI) decontamination efficiency and its adsorbed amount on Fe_3O_4–Cys–PANI vary at different loading levels. There are relatively few surface-active sites at lower doses, causing Cr(VI)-detoxification performance to be irrelevant. However, at an Fe_3O_4–Cys–PANI dose of 0.25 g L^{-1}, the adsorption percentage notably increased to 98.12% due to more available binding sites for Cr(VI) detoxification. Beyond this dose, further increases in the Fe_3O_4–Cys–PANI concentration did not significantly affect the Cr(VI) removal efficiency, likely because the available Cr(VI) ions in the solution became limited relative to the adsorbent surface sites. Therefore, 0.25 g L^{-1} was used for further experiments.

pH effect and mechanism. Both the Cr(VI) solution and the adsorbent's surface charge depend on the pH of the solution, which is paramount in the Cr(VI) adsorption process.[48] The interactions occurring at the interface between these two entities are directly affected by the acidity or basicity of the solution. However, prior to investigating the influence of pH on Cr(VI) adsorption, it is essential to check the adsorbent's surface charge as a function of pH (inset of Fig. 3(b)). The point of zero charge (PZC) value of the Fe_3O_4–Cys–PANI composite was found to be 2.8. This reveals that the surface of the as-prepared Fe_3O_4–Cys–PANI material is positively charged at pH levels below 2.8, while the surface becomes negatively charged at pH levels above 2.8. Hence, a comprehensive study was conducted to evaluate the impact of solution pH on the efficiency of Cr(VI) detoxification using Fe_3O_4–Cys–PANI. The pH values were systematically varied from 2.0 to 10.0 while maintaining consistent experimental conditions: an adsorbent dose of 0.25 g L^{-1}, an initial Cr(VI) concentration of 20 mg L^{-1}, a temperature (T) of 298 K, and a contact time of 90 minutes. Under lower pH conditions, as depicted in Fig. 3(b), the magnetic Fe_3O_4–Cys–PANI material exhibited its maximum potential for detoxifying Cr(VI). It is crucial to consider the various forms of Cr(VI) species present in aqueous solutions within the studied pH range. In acidic media (pH < 6), the predominant species are $HCrO_4^-$ and $Cr_2O_7^{2-}$, which possess strong oxidizing ability and high mobility. As the solution becomes more acidic, the amino groups of the Fe_3O_4–Cys–PANI composite become protonated, resulting in positively charged active sites that enhance the electrostatic attraction of these negatively charged Cr(VI) species (eqn (5) and (6)).[10] This initial adsorption process facilitates the close interaction between the Cr(VI) ions and the redox-active surface of the composite.

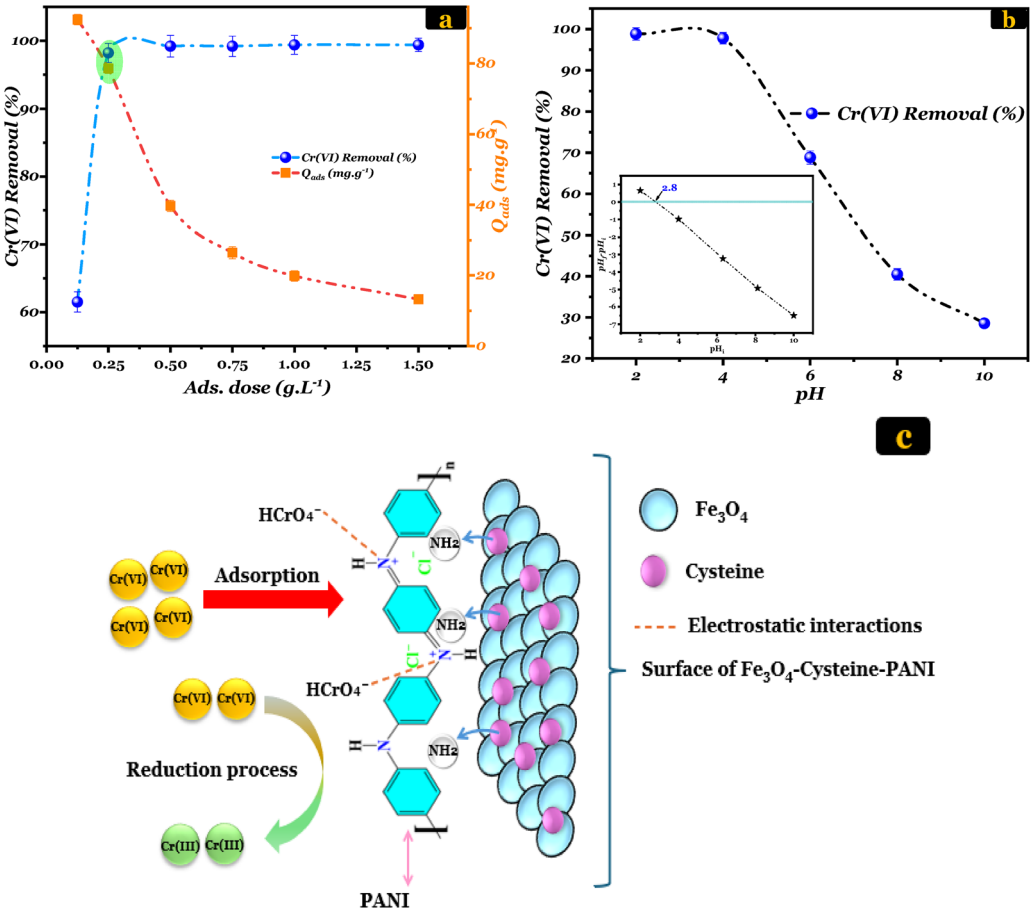

Fig. 3 (a) Effect of adsorbent dosage and (b) effect of pH on Cr(VI) removal. (c) Probable mechanism of Cr(VI) removal.

Subsequently, an *in situ* reduction of Cr(VI) to Cr(III) occurs through electron transfer from the Fe^{2+}/Fe^{3+} redox couple in Fe_3O_4 and from the nitrogen-containing functional groups introduced by cysteine and polyaniline (eqn (7) and (8)).[41,49,50] The presence of cysteine enhances the availability of electron-donating nitrogen sites, while the conjugated structure of PANI promotes charge transfer and electron mobility, both of which accelerate the reduction process. The reduced Cr(III) species, being less toxic and less soluble, can then chelate with amine and imine nitrogen groups on the composite surface, forming stable coordination bonds that prevent their release back into the solution.

$$-NH_3^+ + HCrO_4^- \rightarrow -NH_3^+-HCrO_4^- \quad (5)$$

$$-NH_3^+ + Cr_2O_7^{2-} \rightarrow -NH_3^+-Cr_2O_7^{2-} \quad (6)$$

$$HCrO_4^- + 7H^+ + 3e^- \rightarrow Cr^{3+} + 4H_2O \quad (7)$$

$$Cr_2O_7^{2-} + 14H^+ + 6e^- \rightarrow 2Cr^{3+} + 7H_2O \quad (8)$$

Conversely, at pH = 10, the Cr(VI) removal decreased as the pH values increased. Only 28.57% of Cr(VI) ions were decontaminated using our magnetic composite. Therefore, a pH value of 2 was selected for the subsequent experiments. The schematic representation is provided in Fig. 3(c) for the probable mechanism by which Cr(VI) is adsorbed to the Fe_3O_4–Cys–PANI material.

3.2.2. Adsorption kinetics, isotherm models and comparison

Adsorption kinetics. The contact time of the absorbent and the ability to adsorb quickly are the key features for its successful use in practical applications.[51] The result of adsorbent/adsorbate contact time (from 2 to 180 min) on the decontamination of Cr(VI) oxyanions by the Fe_3O_4–Cys–PANI composite surface was investigated under the following operational conditions: an adsorbent dosage of 0.25 g L^{-1} was used in 100 mL of Cr(VI) solution with initial 20 mg L^{-1} concentration at pH 2 and 25 °C (Fig. 4). A better rate of Cr(VI) oxyanion uptake was noticed when the contact time was increased in the first 30 min, but then it became slower, and equilibrium was attained after 60 min. Accordingly, the removal ability of the Fe_3O_4–Cys–PANI composite was referred to the availability of Cr(VI) oxyanion-binding sites on the Fe_3O_4–Cys–PANI surface. We fit the kinetic data using pseudo-first-order, pseudo-second-order, Elovitch, and intra-particle diffusion kinetic models, and the findings are presented in Fig. 4 and Table 1. According to the table, R^2 of the pseudo-second-order kinetic model was found to be higher than that obtained for others. As the pseudo-second-order kinetic model had a higher correlation with laboratory data, its Q_e value was also similar to the actual experiments' Q_e value.

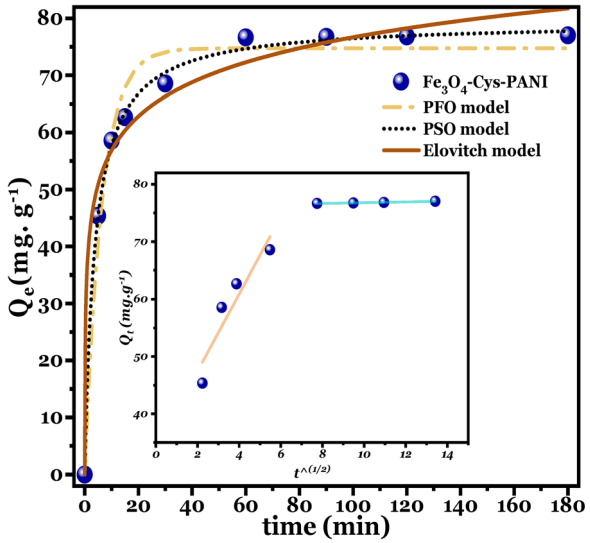

Fig. 4 Pseudo-first-order, pseudo-second-order, Elovitch and Weber–Morris intraparticle diffusion linear plots for Cr(VI) adsorption by Fe_3O_4–Cys–PANI.

The experimental results were further fitted by the intra-particle diffusion kinetic model (inset of Fig. 4). According to the multilinear pattern of the intra-particle diffusion plot, Cr(VI) transfer to solid surfaces is governed by two distinct phases. Initial Cr(VI) ion migration from the aqueous medium to the Fe_3O_4–Cys–PANI composite interface indicates a higher mass flow rate for Cr(VI) ion transfer from the liquid to the absorbent. Adsorption equilibrium is reached after Fe_3O_4–Cys–PANI surface sites are saturated, internal diffusion resistance increases, and the surface sites of the adsorbent are eventually saturated.

Isotherm models. It is a mandatory tool to consider the distribution of Cr(VI) oxyanions from the liquid phase to Fe_3O_4–Cys–PANI (solid phase) up to the equilibrium stage under the controlled (fixed) conditions.[13,51] A pair of conventional adsorption isotherms (Langmuir and Freundlich) have been examined to explain the type of isotherm, the adsorption mechanism, the adsorbent affinity, the reaction nature, whether multilayer or monolayer adsorption, and the maximum capacity of adsorption. Fig. 5(a) and Table 2 show that the Freundlich model anticipates the adsorption of Cr(VI) ions over the Fe_3O_4–Cys–PANI composite better than the Langmuir model, based on the comparison of regression coefficients.

Comparison. Compared with other reported adsorbents, Fe_3O_4–Cys–PANI shows excellent adsorption performance (Fig. 5(b) and Table 3). The literature reports numerous studies on the adsorption of Cr(VI) from water using a variety of materials. The composite exhibits an outstanding maximum uptake capacity of 933.15 mg g^{-1}. Thus, it has the potential to

Table 1 Kinetic and equilibrium parameters of Cr(VI) detoxification on Fe_3O_4–Cys–PANI

	PFO model $Q_t = Q_e(1 - \exp(-k_1 t))$			PSO model $Q_t = \frac{Q_e^2 k_2 t}{1 + Q_e k_2 t}$			Elovitch model $Q_t = \frac{1}{\beta}\ln(\alpha\beta_t)$		
Q_{exp} (mg g^{-1})	k_1	$Q_{e,1}$	R^2	k_2	$Q_{e,2}$	R^2	A	B	R^2
77.98	0.158	74.75	0.981	0.0033	79.35	**0.998**	631.88	0.116	0.982

Weber–Morris model $Q_t = k_{int}t^{1/2} + C$

Initial linear portion		Second linear portion	
$k_{int.1}$	C_1	$k_{int.2}$	C_2
6.731	33.98	0.065	76.14

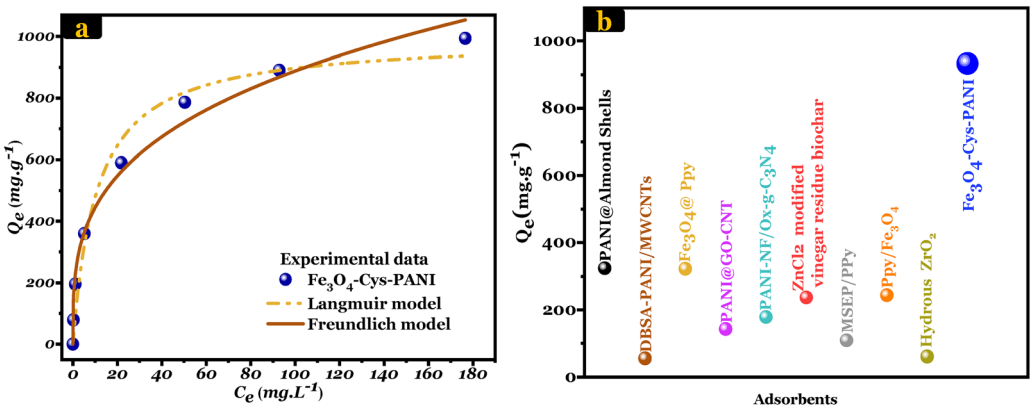

Fig. 5 (a) Non-linear isotherm plots and (b) comparison of our composite with other materials reported in the literature.

Table 2 Isotherm parameters for Cr(VI) decontamination on Fe_3O_4–Cys–PANI

	Langmuir $Q_e = \frac{Q_{max} K_L C_e}{1 + K_L C_e}$			Freundlich $Q_e = K_F C_e^{1/n}$		
Q_{exp} (mg g^{-1})	Q_{max} (mg g^{-1})	K_L (L mg^{-1})	R^2	n_f	K_F (mg g^{-1})	R^2
933.15	994.02	0.097	0.975	3.32	221.95	0.988

be an effective material for removing Cr(VI). Fe_3O_4–Cys–PANI can, therefore, be recommended as a promising and cost-effective wastewater decontamination adsorbent.

3.2.3. Thermodynamic parameters, regeneration and selectivity

Thermodynamics. A study of the temperature effect on the adsorption of Cr(VI) onto Fe_3O_4–Cys–PANI was conducted in order to gain a deeper understanding of the thermodynamic conduct of the adsorption procedure.[61,62] Eqn (9) and (10) were used to evaluate the results:

$$\ln K_d = \frac{\Delta S^\circ}{R} - \frac{\Delta H^\circ}{RT} \quad (9)$$

K_d is the constant distribution equilibrium specified by the following equation:

$$K_d = \frac{Q_e}{C_e} \quad (10)$$

where T (in K), R (8.314 J mol K^{-1}), and ρ (mg L^{-1}) are the absolute temperature, universal gas constant, and water density, respectively.

As part of this research, the Cr(VI) adsorption by Fe_3O_4–Cys–PANI was examined at three different temperatures: 298 K, 308 K and 318 K (Fig. 6(a) and Table 4). From the experimental data, standard thermodynamic parameters were estimated for understanding the thermodynamic behavior. It can be demonstrated that the ΔG° values are negative, provided that the removal of Cr(VI) occurred spontaneously onto the Fe_3O_4–Cys–PANI surface sites. Furthermore, the gradual decrease in the absolute values of ΔG° as the temperature increases suggests that higher temperatures are more favorable to global adsorption. The positive ΔH° value suggests that the adsorption of Cr(VI) onto Fe_3O_4–Cys–PANI is an endothermic process. This is supported by the positive ΔS° value, indicating the strong affinity of Fe_3O_4–Cys–PANI surfaces for Cr(VI) ions at the adsorbent–adsorbate interface.

Regeneration. The critical factor in assessing the practical applications of the designed adsorbent lies in its regeneration potential.[10,63] After the adsorption test, the recovered Fe_3O_4–Cys–PANI was reutilized for five runs, as shown in Fig. 6(b). The efficiency of Cr(VI) decontamination using Fe_3O_4–Cys–PANI provides excellent regenerability and outstanding reusability. This suggests that Fe_3O_4–Cys–PANI maintains its adsorption performance even after multiple regeneration runs, making it a promising candidate for practical applications in water treatment.

Selectivity. There is no doubt that wastewater is polluted by heavy metals and other organic and inorganic pollutants as well.[55,64] Therefore, assessing the influence of co-interfering ions is necessary. Herein, a series of adsorption tests were performed, maintaining the Cr(VI) concentration at 20 mg L^{-1} and the concentrations of co-interfering ions (CO_3^{2-}, SO_4^{2-}, and NO_3^-) at 100 mg L^{-1}. As shown in Fig. 6(c), the presence of CO_3^{2-} and NO_3^- ions did not impact the decontamination of Cr(VI). However, SO_4^{2-} ions caused a slight decline of 2.5%. This indicates the selectivity of the Fe_3O_4–Cys–PANI composite in detoxifying Cr(VI) oxyanions. Furthermore, the adsorption behavior of Fe_3O_4–Cys–PANI was tested with three pollutants: orange G dye (OG), methylene blue dye (MB), and 4-nitrophenol (4-NP) (Fig. 6(d)). The results showed that Fe_3O_4–Cys–PANI achieved an impressive decontamination rate of over 94% for Cr(VI) oxyanions, with an adsorption capacity around 933.15 mg g^{-1}, whereas the adsorption rates for the other pollutants were below 60%. Compared to the other pollutants, Fe_3O_4–Cys–PANI has a higher selectivity for Cr(VI).

3.3. Theoretical results

3.3.1. DFT insight: Frontier molecular orbitals for the cysteine molecule. The optimized structure by the PBE-6-311++g(d,p) level of theory, the frontier molecular orbitals (HOMO and LUMO), the electrostatic potential map (ESP map), as well as the electronic characteristic aspects in the solvent cavity, which are examined to ascertain the characteristics of cysteine and shed light on its reactivity. The comprehension of the structural influences on the reactivity of cysteine

Table 3 Comparison of the adsorption performance of Fe_3O_4–Cys–PANI for Cr(VI) with previously reported materials

		Operating conditions			
Adsorbent	Q_{max} (mg g^{-1})	Conc (mg L^{-1})	Ads. dose (g L^{-1})	pH	Ref.
Polyaniline@almond shells	324.48	100–400	2	4.5	52
DBSA-PANI/MWCNTs	55.55	20–140	1.33	2	53
Fe_3O_4@polypyrrol	322.58	50–450	1	2	54
PANI@graphene oxide-CNT	142.86	25–200	1	2	55
polyaniline-NF/Ox-g-C_3N_4	178.57	25–300	0.6	2	56
$ZnCl_2$ modified vinegar residue biochar	236.8	10–1500	2	2	57
MSEP/PPy	108.85	10–100	0.5	2	58
Polypyrrole/Fe_3O_4 magnetic nanocomposite	169.4–243.9	200–600	2	2	59
Hydrous zirconium oxide	61	100–200	2	2	60
Fe_3O_4–Cys–PANI	**933.15**	**20–500**	**0.25**	**2**	**Current study**

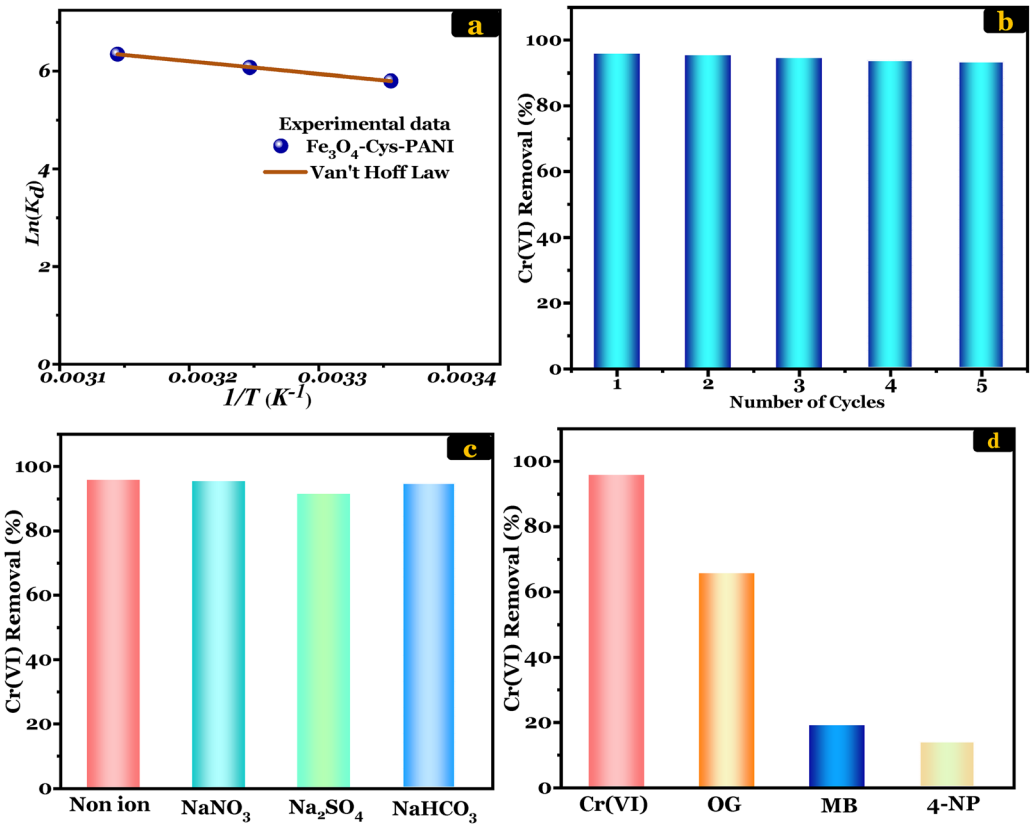

Fig. 6 (a) van't Hoff law plot. (b) Regeneration cycles. (c) Effect of co-interfering ions. (d) Selectivity towards orange G (OG), methylene blue (MB) dyes and 4-nitrophenol (4-NP).

Table 4 Thermodynamic parameters related to Cr(VI) adsorption onto the Fe_3O_4–Cys–PANI surface

		ΔG° (kJ mol^{-1})		
ΔH° (kJ mol^{-1})	ΔS° (J mol^{-1} K^{-1})	298 K	308 K	318 K
30.973	17.361	−14.37	−15.56	−16.77

in its isolated form requires a comprehension of such fundamental concepts. The helpfulness of chemical reactivity in the adsorption and removal studies of heavy metals especially Cr(VI) ions has been well established as complementary to experimental studies.[65–68] Herein, the main aim of the current study is to remove Cr(VI) from wastewater using the Fe_3O_4–Cys–PANI hybrid composite, for which the neutral form of the cysteine is considered.

The optimized molecular structure, 3D representation of HOMO and LUMO and ESP map are shown in Fig. 7. The HOMO and LUMO (E_{HOMO} and E_{LUMO}) energies belong to the popular quantum chemical descriptors.[69–72] As stated previously, the HOMO corresponds to the area in a molecule that can donate electrons (electron-rich region) to the adsorbent surface, while the LUMO specifies the region within the molecule (electron-poor region) that tends to accept electrons from the adsorbent during the adsorption process.[73] The figure reveals that the carboxylic group, linked to the thiol group, forms an angle of approximately 5° with the remaining part of the molecule, indicating that the native configuration of cysteine is nearly planar. This molecule's planarity may be crucial when considering how cysteine interacts with PANI and the Fe_3O_4–Cys–PANI composite. According to a report, the planar structure can offer a greater surface area for interaction with the Fe_3O_4 combination.[74,75]

3.3.2. Understanding adsorption through a theoretical study. Comprehending the adsorption energies assists in uncovering the fundamental mechanisms and facilitates the creation of efficient adsorption strategies for Cr(VI) ions on the Fe_3O_4–Cys–PANI hybrid composite surface.[72,76–78] The purpose of the Monte Carlo/SA simulations was to get an atomic-scale insight into the mechanism and strength of the Cr(VI) ion's adsorption process over the Fe_3O_4–Cys–PANI hybrid composite. Theoretical calculations and interpretation of the surface-related adsorption energies reveal that the (110) face, which makes up 55.17% of the crystal surface, has a higher percentage of total facet area,[79] indicating that it was the primary face where the Cr(VI) ion adsorption process took place. The (110) face was chosen as a representative Fe_3O_4 surface model for the adsorption study.

The adsorption of cysteine on the Fe_3O_4 surface was quantitatively inspected by calculating the adsorption energy (E_{Ads}, eqn (10)), which is the energy necessary during the adsorption of cysteine on the Fe_3O_4 Surface. According to the equilibrium

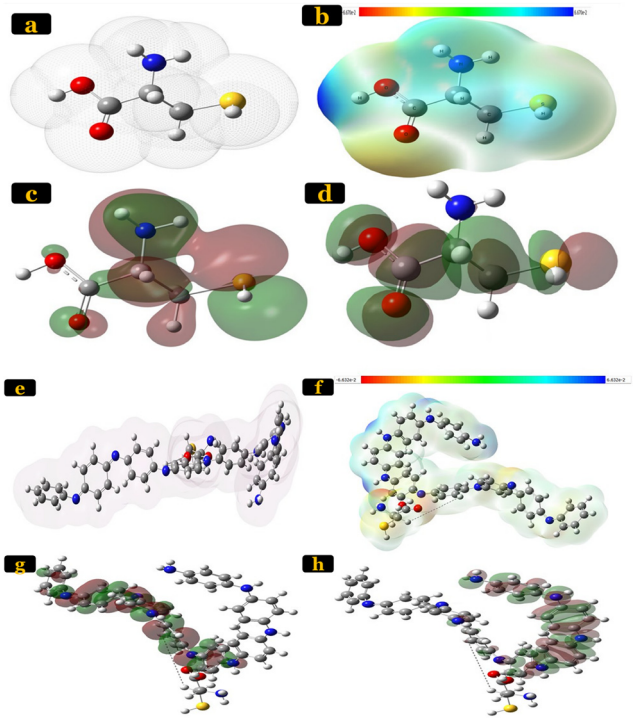

Fig. 7 (a) Optimized structures of cysteine with the solvent cavity; 3D-isosurface visualization of (b) ESP map, (c) LUMO, and (d) HOMO map; (e) optimized structures of Cys–PANI with the solvent cavity; 3D-isosurface visualization of (f) ESP map, (g) LUMO and (h) HOMO map as obtained using DFT at the PBE/6-311++g(d,p) level of theory in aqueous solutions using the IEFPCM solvation model. For HOMO and LUMO surfaces, green and tan colors correspond to positive and negative potentials, respectively. For ESP, the color grades are shown under each map.

configurations shown in Fig. 8, the adsorption energy (E_{ads} = −91.681 kcal mol^{-1}) was achieved by carrying out MC calculations. Furthermore, cysteine was situated about parallel to the surface of Fe_3O_4. The large negative value of the adsorption energy for Fe_3O_4–Cys inferred that the adsorption was exothermic and stable, and this composite was formed through the sp^3 nitrogen atom of cysteine and Fe_3O_4 in a flat mode as well as hydrogen bonds.

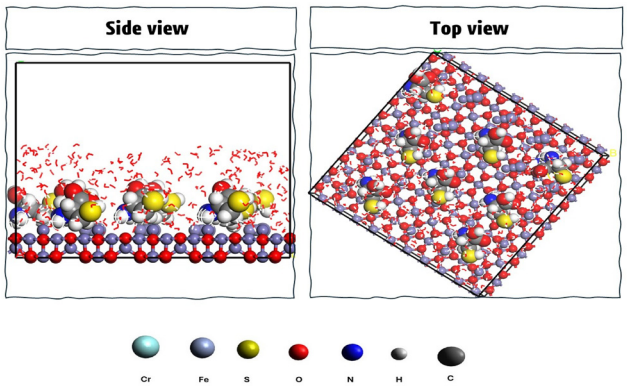

Fig. 8 Equilibrated adsorption configuration of cysteine on Fe_3O_4 surfaces in the aqueous phase, on side and top views.

According to the obtained results, the values of adsorption energy of PANI are largely negative, suggesting spontaneous adsorption of PANI on Fe_3O_4–Cys (E_{ads} = −165.6 kcal mol^{-1}), inferring that the physisorption could lead to the formation of a new composite that was reactive and exothermic. PANI molecules were located in the parallel position on Fe_3O_4–Cys (Fig. 9). If we consider the Cys–PANI interaction, the unprotonated oxygen and oxygen sp^2 atoms of cysteine were directed toward the PANI molecules, involving its favorable interaction with it, as displayed in Fig. 9. The remarkable adsorption capacity of PANI on Fe_3O_4–Cys was attributed to strong interactions of PANI molecules on the Fe_3O_4–Cys surface to produce a Fe_3O_4–Cys–PANI hybrid composite.

To further understand the adsorption behavior observed at different pH levels, it is essential to investigate the interaction energy between Cr(VI) ions and the Fe_3O_4–Cys–PANI interface. In this regard, experimental findings were supplemented with theoretical simulations to gain a deeper understanding of adsorption mechanisms. The interaction between the adsorbate ion and the interface of Fe_3O_4–Cys and polyaniline (PANI) is a significant source of valuable information. By analyzing this interaction, adsorption energies associated with this method may be calculated, providing crucial insights into the system's energy and durability. MC/SA simulation was used to elucidate the adsorption of Cr(VI) ions in the aqueous phase, and the results are exhibited in Fig. 10 by considering the aqueous system during this simulation, the adsorption energy of Cr(VI) ions on Fe_3O_4–Cys–PANI was calculated to be E_{ads} = −55.613 kcal mol^{-1}. Because the Monte Carlo simulation produced such a negative result, it validated experimental findings, and the process was stable and spontaneous, and Cr(VI) can be effectively adsorbed on Fe_3O_4–Cys–PANI.[80,81] According to this figure, the adsorption orientation of Cr(VI) ions is strongly influenced by the chemical nature of the Fe_3O_4–Cys–PANI substrate. The calculated distance between the nitrogen atom of the cysteine moiety and the chromate ion is approximately 2.96 Å, while the distance between the nitrogen atom of the polyaniline heterocycle and the chromate ion is around 3.07 Å. In contrast, the distance between the ferric ion of Fe_3O_4 and the chromium atom is noticeably shorter, indicating stronger interactions and distinct reactivities among the

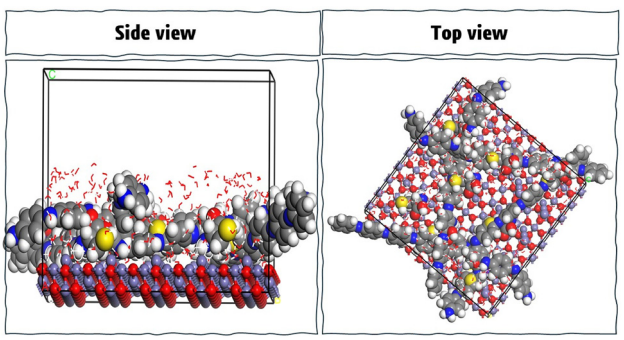

Fig. 9 Side and top views for the lowest energy geometries derived from MC for the PANI molecules adsorbed onto the interface of Fe_3O_4–Cys.

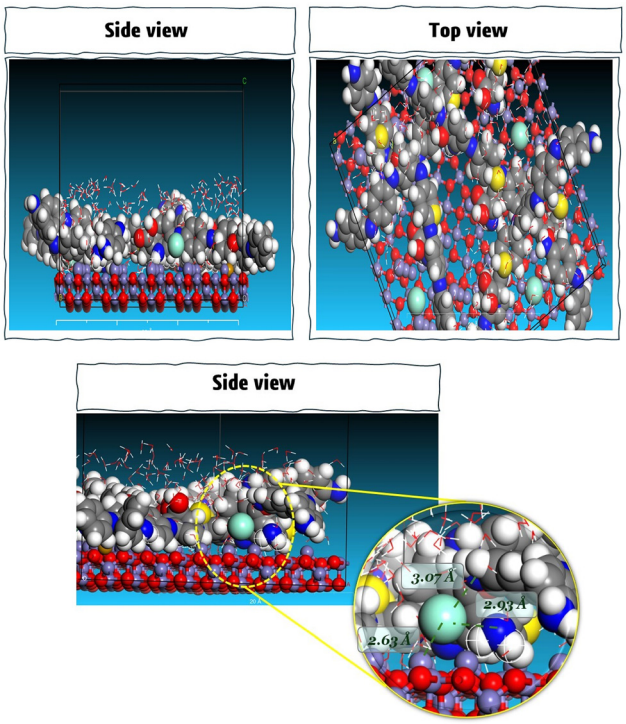

Fig. 10 The side and top views of the stable adsorption configuration of Cr(VI) ions on Fe_3O_4–Cys–PANI surfaces under solvation conditions.

active sites. These results suggest that electrostatic interactions initially guide and pre-orient the chromate ions near the surface, facilitating subsequent strong bonding and contributing to the overall stability of the adsorbed complex. Furthermore, the Fe_3O_4–Cys–PANI system exhibited the lowest adsorption energy, confirming its enhanced affinity and stability toward Cr(VI) species.[82,83] This suggested that the Cr(VI) ion's adsorption process was more robust, steady, and spontaneous on the Fe_3O_4–Cys–PANI system. Therefore, this provided a good clarification for why the elimination efficiency of Cr ion was improved after the use of the Fe_3O_4–Cys–PANI hybrid composite.[72,84]

4. Conclusion

To sum up, the magnetic Fe_3O_4–Cys–PANI composite was successfully synthesized and characterized, exhibiting tunable properties for efficient Cr(VI) detoxification. The functionalization with cysteine introduced N-containing groups that enhanced the surface reactivity and facilitated the interaction with Cr(VI) species. The magnetic adsorbent achieved a maximum Cr(VI) removal efficiency of 98.12% at an adsorbent dose of 0.25 $g{\cdot}L^{-1}$ and pH 2, where acidic conditions favored both the reduction of Cr(VI) to Cr(III) and the adsorption of $Cr_2O_7^{2-}$ and $HCrO_4^-$ ions through electrostatic attraction. Monte Carlo simulations revealed a high adsorption energy of -55.613 $kcal{\cdot}mol^{-1}$, confirming the strong binding affinity between Cr(VI) species and the active sites of Fe_3O_4–Cys–PANI, in agreement with experimental observations. Freundlich isotherm and pseudo-second-order kinetic models accurately described the Cr(VI) decontamination behavior. Moreover, the Fe_3O_4–Cys–PANI magnetic composite demonstrated exceptional selectivity towards Cr(VI) oxyanions and significant regeneration capacities and reusability as well. Although this study presents promising results in depolluting Cr(VI) solutions under controlled conditions, further work is needed to evaluate the economic feasibility of the tailored Fe_3O_4–Cys–PANI composite in real wastewater treatment applications.

Author contributions

A. Imgharn: formal analysis, data curation, writing – original draft; M. El Houdi: formal analysis, writing – original draft; S. El Omari: methodology, data curation; K. Ait El Bacha: investigation; M. Laabd: validation, review & editing; L. Bazzi: validation, review & editing; A. Albourine: conceptualization, validation, revision, editing, supervision, project administration.

Conflicts of interest

The authors declare that they have no known competing financial interests or personal relationships that could have appeared to influence the work reported in this paper.

Data availability

The data for this article are available from the corresponding author.

Acknowledgements

The authors received no specific funding for this work.

References

1 Z. Rahman and L. Thomas, Chemical-Assisted Microbially Mediated Chromium (Cr)(VI) Reduction Under the Influence of Various Electron Donors, Redox Mediators, and Other Additives: An Outlook on Enhanced Cr(VI) Removal, *Front. Microbiol.*, 2021, **11**, 619766, DOI: 10.3389/fmicb.2020.619766.
2 L. Wang, Y. Wang, F. Ma, V. Tankpa, S. Bai, X. Guo and X. Wang, Mechanisms and Reutilization of Modified Biochar Used for Removal of Heavy Metals from Wastewater: A Review, *Sci. Total Environ.*, 2019, **668**, 1298–1309, DOI: 10.1016/j.scitotenv.2019.03.011.
3 J. Liang, X. Huang, J. Yan, Y. Li, Z. Zhao, Y. Liu, J. Ye and Y. Wei, A Review of the Formation of Cr(VI) *via* Cr(III) Oxidation in Soils and Groundwater, *Sci. Total Environ.*, 2021, **774**, 145762, DOI: 10.1016/j.scitotenv.2021.145762.
4 R. Zheng, J. Li, R. Zhu, R. Wang, X. Feng, Z. Chen, W. Wei, D. Yang and H. Chen, Enhanced Cr(VI) Reduction on Natural Chalcopyrite Mineral Modulated by Degradation Intermediates of RhB, *J. Hazard. Mater.*, 2022, **423**, 127206, DOI: 10.1016/j.jhazmat.2021.127206.

5 P. Sharma, S. P. Singh, S. K. Parakh and Y. W. Tong, Health Hazards of Hexavalent Chromium (Cr(VI)) and Its Microbial Reduction, *Bioengineered*, 2022, **13**(3), 4923–4938, DOI: 10.1080/21655979.2022.2037273.

6 A. Imgharn, M. Laabd, Y. Naciri, A. Hsini, F.-Z. Mahir, H. Zouggari and A. Albourine, Insights into the Performance and Mechanism of PANI@Hydroxapatite-Montmorillonite for Hexavalent Chromium Cr(VI) Detoxification, *Surf. Interfaces*, 2023, **36**, 102568, DOI: 10.1016/j.surfin.2022.102568.

7 B. Kumari, R. K. Tiwary and M. Yadav, Non Linear Regression Analysis and RSM Modeling for Removal of Cr(VI) from Aqueous Solution Using PANI@WH Composites, *Mater. Chem. Phys.*, 2022, **290**, 126457, DOI: 10.1016/j.matchemphys.2022.126457.

8 L. Xiang, C.-G. Niu, N. Tang, X.-X. Lv, H. Guo, Z.-W. Li, H.-Y. Liu, L.-S. Lin, Y.-Y. Yang and C. Liang, Polypyrrole Coated Molybdenum Disulfide Composites as Adsorbent for Enhanced Removal of Cr(VI) in Aqueous Solutions by Adsorption Combined with Reduction, *Chem. Eng. J.*, 2021, **408**, 127281, DOI: 10.1016/j.cej.2020.127281.

9 R. Ansari and A. Fallah Delavar, Removal of Cr(VI) Ions from Aqueous Solutions Using Poly 3-Methyl Thiophene Conducting Electroactive Polymers, *J. Polym. Environ.*, 2010, **18**(3), 202–207, DOI: 10.1007/s10924-010-0199-7.

10 M. Laabd, A. Imgharn, A. Hsini, Y. Naciri, M. Mobarak, S. Szunerits, R. Boukherroub and A. Albourine, Efficient Detoxification of Cr(VI)-Containing Effluents by Sequential Adsorption and Reduction Using a Novel Cysteine-Doped PANi@faujasite Composite: Experimental Study Supported by Advanced Statistical Physics Prediction, *J. Hazard. Mater.*, 2022, **422**, 126857, DOI: 10.1016/j.jhazmat.2021.126857.

11 J. Qiu, F. Liu, S. Cheng, L. Zong, C. Zhu, C. Ling and A. Li, Recyclable Nanocomposite of Flowerlike MoS_2@Hybrid Acid-Doped PANI Immobilized on Porous PAN Nanofibers for the Efficient Removal of Cr(VI), *ACS Sustainable Chem. Eng.*, 2018, **6**(1), 447–456, DOI: 10.1021/acssuschemeng.7b02738.

12 M. H. Mahmoudian, A. Azari, A. Jahantigh, M. Sarkhosh, M. Yousefi, S. A. Razavinasab, M. Afsharizadeh, F. Mohammadi Shahraji, A. Pour Pasandi, A. Zeidabadi, T. Ilaghinezhad Bardsiri and M. Ghasemian, Statistical Modeling and Optimization of Dexamethasone Adsorption from Aqueous Solution by Fe_3O_4@NH_2-MIL88B Nanorods: Isotherm, Kinetics, and Thermodynamic, *Environ. Res.*, 2023, **236**, 116773, DOI: 10.1016/j.envres.2023.116773.

13 R.-S. Juang, Y.-C. Yei, C.-S. Liao, K.-S. Lin, H.-C. Lu, S.-F. Wang and A.-C. Sun, Synthesis of Magnetic Fe_3O_4/Activated Carbon Nanocomposites with High Surface Area as Recoverable Adsorbents, *J. Taiwan Inst. Chem. Eng.*, 2018, **90**, 51–60, DOI: 10.1016/j.jtice.2017.12.005.

14 Y.-F. Lin and C.-Y. Chang, Magnetic Mesoporous Iron Oxide/Carbon Aerogel Photocatalysts with Adsorption Ability for Organic Dye Removal, *RSC Adv.*, 2014, **4**(54), 28628, DOI: 10.1039/c4ra03436h.

15 A. Nasiri, M. A. Gharaghani, G. Yazdanpanah, H. Mahdizadeh and N. Amirmahani, Facile, Fast, and Green Synthesis of $CoFe_2O_4$@CMC/Cysteine as a Novel Magnetic Nanobiocomposite Adsorbent for Tetracycline Removal from Aqueous Media, *J. Polym. Environ.*, 2025, **33**(9), 4212–4236, DOI: 10.1007/s10924-025-03629-x.

16 S. Abolghasemi, A. Nasiri, M. Hashemi, S. Rajabi and F. Rahimi, Magnetic Nanocomposites: Innovative Adsorbents for Antibiotics Removal from Aqueous Environments–a Narrative Review, *Appl. Water Sci.*, 2025, **15**(2), 30, DOI: 10.1007/s13201-025-02360-1.

17 S. Rajabi, H. Hashemi, M. R. Samaei, A. Nasiri, A. Azhdarpoor and S. Yousefinejad, Enhanced Sonophoto-Catalytic and Adsorption Capabilities of Fe_3O_4@MC/MWCNT-CuO/Ag for Petrochemical Organic Pollutants Degradation from Industrial Process Streams, *Arabian J. Chem.*, 2024, **17**(11), 105994, DOI: 10.1016/j.arabjc.2024.105994.

18 T. T. H. Chu and M. V. Nguyen, Improved Cr(VI) Adsorption Performance in Wastewater and Groundwater by Synthesized Magnetic Adsorbent Derived from Fe3O4 Loaded Corn Straw Biochar, *Environ. Res.*, 2023, **216**, 114764, DOI: 10.1016/j.envres.2022.114764.

19 A. Pasgar, A. Nasiri and N. Javid, Single and Competitive Adsorption of Cu^{2+} and Pb^{2+} by Tea Pulp from Aqueous Solutions, *Environ. Health Eng. Manage. J.*, 2021, **9**(1), 65–74, DOI: 10.34172/EHEM.2022.08.

20 A. Imgharn, L. Anchoum, A. Hsini, Y. Naciri, M. Laabd, M. Mobarak, N. Aarab, A. Bouziani, S. Szunerits, R. Boukherroub, R. Lakhmiri and A. Albourine, Effectiveness of a Novel polyaniline@Fe-ZSM-5 Hybrid Composite for Orange G Dye Removal from Aqueous Media: Experimental Study and Advanced Statistical Physics Insights, *Chemosphere*, 2022, **295**, 133786, DOI: 10.1016/j.chemosphere.2022.133786.

21 R. Dennington; T. A. Keith and J. M. Millam, *GaussView, Version 6.0. 16.*, Semichem Inc, Shawnee Mission KS, 2016.

22 E. Caldeweyher, C. Bannwarth and S. Grimme, Extension of the D3 Dispersion Coefficient Model, *J. Chem. Phys.*, 2017, **147**(3), 034112, DOI: 10.1063/1.4993215.

23 P. J. Hay and W. R. Wadt, *Ab Initio* Effective Core Potentials for Molecular Calculations. Potentials for the Transition Metal Atoms Sc to Hg, *J. Chem. Phys.*, 1985, **82**(1), 270–283, DOI: 10.1063/1.448799.

24 M. N. Rasul, A. Anam, M. A. Sattar, A. Manzoor and A. Hussain, DFT Based Structural, Electronic and Optical Properties of $B_{1-x}In_xP$ (x = 0.0, 0.25, 0.5, 0.75, 1.0) Compounds: PBE-GGA *vs.* mBJ-Approaches, *Chin. J. Phys.*, 2018, **56**(6), 2659–2672.

25 M. Arshad Javid, Z. U. Khan, Z. Mehmood, A. Nabi, F. Hussain, M. Imran, M. Nadeem and N. Anjum, Structural, Electronic and Optical Properties of $LiNbO_3$ Using GGA-PBE and TB-mBJ Functionals: A DFT Study, *Int. J. Mod. Phys. B*, 2018, **32**(14), 1850168.

26 M. Elhoudi, N. Aarab and M. Laabd, Quantum Chemical Approach (DFT) of the Binary Complexation of Hg(II), *Moroccan J. Chem.*, 2021, **3**, 406–415.

27 M. J. Frisch; G. W. Trucks; H. B. Schlegel; G. E. Scuseria; M. A. Robb; J. R. Cheeseman; G. Scalmani; V. Barone; G. A. Petersson; H. Nakatsuji; X. Li; M. Caricato; A. Marenich; J. Bloino; B. G. Janesko; R. Gomperts; B. Mennucci;

H. P. Hratchian; J. V. Ortiz; A. F. Izmaylov; J. L. Sonnenberg; D. Williams-Young; F. Ding; F. Lipparini; F. Egidi; J. Goings; B. Peng; A. Petrone; T. Henderson; D. Ranasinghe; V. G. Zakrzewski; J. Gao; N. Rega; G. Zheng; W. Liang; M. Hada; M. Ehara; K. Toyota; R. Fukuda; J. Hasegawa; M. Ishida; T. Nakajima; Y. Honda; O. Kitao; H. Nakai; T. Vreven; K. Throssell; J. A. Montgomery Jr.; J. E. Peralta; F. Ogliaro; M. Bearpark; J. J. Heyd; E. Brothers; K. N. Kudin; V. N. Staroverov; T. Keith; R. Kobayashi; J. Normand; K. Raghavachari; A. Rendell; J. C. Burant; S. S. Iyengar; J. Tomasi; M. Cossi; J. M. Millam; M. Klene; C. Adamo; R. Cammi; J. W. Ochterski; R. L. Martin; K. Morokuma; O. Farkas; J. B. Foresman and D. J. Fox, *Gaussian 09, Rev. D.01*, Gaussian Inc., Wallingford, CT, 2016.

28 M. Cossi; N. Rega; G. Scalmani; V. Barone; D. Chimica; F. Ii and C. M. S. Angelo Molecules in Solution with the C-PCM Solvation Model. 2003.

29 A. P. Scott and L. Radom, Harmonic Vibrational Frequencies: An Evaluation of Hartree-Fock, Møller-Plesset, Quadratic Configuration Interaction, Density Functional Theory, and Semiempirical Scale Factors, *J. Phys. Chem.*, 1996, **100**(41), 16502–16513, DOI: **10.1021/jp960976r**.

30 S. Baroni, P. Giannozzi and E. Isaev, Density-Functional Perturbation Theory for Quasi-Harmonic Calculations, *Rev. Mineral. Geochem.*, 2010, **71**(1), 39–57.

31 S. Kirkpatrick, C. D. Gelatt Jr and M. P. Vecchi, Optimization by Simulated Annealing, *Science*, 1983, **220**(4598), 671–680.

32 P. J. M. Van Laarhoven; E. H. L. Aarts; P. J. M. van Laarhoven and E. H. L. Aarts, *Simulated Annealing*, Springer, 1987.

33 National Center for Biotechnology Information (2025). PubChem Substance Record for SID 85240249, 25233-30-1, Source: ChEBI. Retrieved February 19, 2025 from **https://pubchem.ncbi.nlm.nih.gov/substance/85240249**. No Title.

34 I. A. M. Ahmed and B. A. Maher, Identification and Paleoclimatic Significance of Magnetite Nanoparticles in Soils, *Proc. Natl. Acad. Sci. U. S. A.*, 2018, **115**(8), 1736–1741, DOI: **10.1073/pnas.1719186115**.

35 I. B. Obot, K. Haruna and T. A. Saleh, Atomistic Simulation: A Unique and Powerful Computational Tool for Corrosion Inhibition Research, *Arabian J. Sci. Eng.*, 2019, **44**, 1–32.

36 Materials Studio. Accelrys Software Inc., S. Diego. N. that; 2, some of these codes were also offered as part of the C.; From, application that preceded M. S. 2013. No Title.

37 B. Vellaichamy and P. Periakaruppan, Synergistic Combination of a Novel Metal-Free Mesoporous Band-Gap-Modified Carbon Nitride Grafted Polyaniline Nanocomposite for Decontamination of Refractory Pollutant, *Ind. Eng. Chem. Res.*, 2018, **57**(19), 6684–6695, DOI: **10.1021/acs.iecr.8b01098**.

38 X. Song, C. Ren, Q. Zhao and B. Su, Simultaneous Removal of Cr(VI) and Triclosan from Aqueous Solutions through Fe_3O_4 Magnetic Nanoscale-Activated Persulfate Oxidation, *Chem. Eng. J.*, 2020, **381**, 122586, DOI: **10.1016/j.cej.2019.122586**.

39 I. M. Minisy, N. A. Salahuddin and M. M. Ayad, Adsorption of Methylene Blue onto Chitosan–Montmorillonite/Polyaniline Nanocomposite, *Appl. Clay Sci.*, 2021, **203**, 105993, DOI: **10.1016/j.clay.2021.105993**.

40 A. Nasiri, M. R. Heidari, N. Javid and G. Yazdanpanah, New Efficient and Recyclable Magnetic Nanohybrid Adsorbent for the Metronidazole Removal from Simulated Wastewater, *J. Mater. Sci.: Mater. Electron.*, 2022, **33**(33), 25103–25126, DOI: **10.1007/s10854-022-09216-3**.

41 A. Chaoui, A. Imgharn, A. C. Estrada, A. B. Hamou, S. Farsad, N. Nouj, M. Ez-zahery, T. Trindade, A. Albourine and N. E. Alem, Chromium (VI) Remediation *via* Biochar@-polyaniline Composite: Advancing Water Treatment Using Biogas Residue Digestate, *Adv. Compos. Hybrid Mater.*, 2025, **8**(4), 312, DOI: **10.1007/s42114-025-01345-7**.

42 S. El Omari, A. Imgharn, Y. Abdellaoui, O. May Tzuc, A. Albourine, L. Bazzi, M. Laabd and K. Benhabib, A Hybrid Polyaniline/Dolomite–Palygorskite Framework for Environmental Remediation: Experimental Design and Molecular-Level Adsorption Interpretation, *Mater. Adv.*, 2025, **6**(20), 7409–7426, DOI: **10.1039/D5MA00660K**.

43 Astuti, S. Arief, M. Muldarisnur, Zulhadjri and S. R. A. Usna, Enhancement in Photoluminescence Performance of Carbon-Based Fe_3O_4@ZnO–C Nanocomposites, *Vacuum*, 2023, **211**, 111935, DOI: **10.1016/j.vacuum.2023.111935**.

44 S. Song, X. Qiu, S. Huang, H. Tian, R. Pu, J. Huang, J. Su, Y.-L. Tang, L. Huang, X. Luo, W. He, Q. Ni and W. Zhang, Cystine-Modified Lignin–Copper Coordination Nanocarriers Improve the Therapeutic Efficacy of Tyrosine Kinase Inhibition *via* Cuproptosis, *ACS Appl. Mater. Interfaces*, 2025, **17**(6), 9074–9086, DOI: **10.1021/acsami.4c20305**.

45 A. Cervellino; R. Frison; N. Masciocchi and A. Guagliardi, X-Ray Powder Diffraction Characterization of Nanomaterials, in *X-ray and Neutron Techniques for Nanomaterials Characterization*, ed. C. S. S. R. Kumar, Springer Berlin Heidelberg, Berlin, Heidelberg, 2016, pp 545–608, DOI: **10.1007/978-3-662-48606-1_10**.

46 A. Imgharn, T. Sun, J. Nicolle, Y. Naciri, A. Hsini, A. Albourine and C. Ania, A Simple Approach to Prepare a C_3N_4/MoO_3 Heterojunction with Improved Photocatalytic Performance for the Degradation of Methylparaben, *Catalysts*, 2024, **14**(3), 170, DOI: **10.3390/catal14030170**.

47 A. L. Patterson, The Scherrer Formula for X-Ray Particle Size Determination, *Phys. Rev.*, 1939, **56**(10), 978–982, DOI: **10.1103/PhysRev.56.978**.

48 Q. Wang, L. Li, Y. Tian, L. Kong, G. Cai, H. Zhang, J. Zhang, W. Zuo and B. Wen, Shapeable Amino-Functionalized Sodium Alginate Aerogel for High-Performance Adsorption of Cr(VI) and Cd(II): Experimental and Theoretical Investigations, *Chem. Eng. J.*, 2022, **446**, 137430, DOI: **10.1016/j.cej.2022.137430**.

49 W. Wang, C. Chen, X. Huang, S. Jiang, J. Xiong, J. Li, M. Hong, J. Zhang, Y. Guan, X. Feng, W. Tan, F. Liu, L.-J. Ding and H. Yin, Chromium(VI) Adsorption and Reduction in Soils under Anoxic Conditions: The Relative Roles of Iron (Oxyhr)Oxides, Iron(II), Organic Matters, and Microbes, *Environ. Sci. Technol.*, 2024, **58**(41), 18391–18403, DOI: **10.1021/acs.est.4c08677**.

50 A. Hsini, R. Haounati, A. Imgharn, Y. Naciri, R. E. Malekshah, A. Shaim, S. Szunerits, R. Boukherroub and A. Albourine, 1,2,4,5-Benzene Tetracarboxylic Acid-Doped Polyaniline/Protonated Carbon Nitride Nanostructures for Cr(VI) Adsorption in Water, *ACS Appl. Nano Mater.*, 2024, **7**(11), 13050–13061, DOI: **10.1021/acsanm.4c01503**.

51 F.-X. Dong, L. Yan, X.-H. Zhou, S.-T. Huang, J.-Y. Liang, W.-X. Zhang, Z.-W. Guo, P.-R. Guo, W. Qian, L.-J. Kong, W. Chu and Z.-H. Diao, Simultaneous Adsorption of Cr(VI) and Phenol by Biochar-Based Iron Oxide Composites in Water: Performance, Kinetics and Mechanism, *J. Hazard. Mater.*, 2021, **416**, 125930, DOI: **10.1016/j.jhazmat.2021.125930**.

52 A. Hsini, A. Essekri, N. Aarab, M. Laabd, A. Ait Addi, R. Lakhmiri and A. Albourine, Elaboration of Novel polyaniline@Almond Shell Biocomposite for Effective Removal of Hexavalent Chromium Ions and Orange G Dye from Aqueous Solutions, *Environ. Sci. Pollut. Res.*, 2020, **27**(13), 15245–15258, DOI: **10.1007/s11356-020-08039-1**.

53 R. Kumar, M. O. Ansari and M. A. Barakat, DBSA Doped Polyaniline/Multi-Walled Carbon Nanotubes Composite for High Efficiency Removal of Cr(VI) from Aqueous Solution, *Chem. Eng. J.*, 2013, **228**, 748–755, DOI: **10.1016/j.cej.2013.05.024**.

54 M. Chigondo, H. K. Paumo, M. Bhaumik, K. Pillay and A. Maity, Magnetic Arginine-Functionalized Polypyrrole with Improved and Selective Chromium(VI) Ions Removal from Water, *J. Mol. Liq.*, 2019, **275**, 778–791, DOI: **10.1016/j.molliq.2018.11.032**.

55 M. O. Ansari, R. Kumar, S. A. Ansari, S. P. Ansari, M. A. Barakat, A. Alshahrie and M. H. Cho, Anion Selective pTSA Doped Polyaniline@graphene Oxide-Multiwalled Carbon Nanotube Composite for Cr(VI) and Congo Red Adsorption, *J. Colloid Interface Sci.*, 2017, **496**, 407–415, DOI: **10.1016/j.jcis.2017.02.034**.

56 R. Kumar, M. A. Barakat and F. A. Alseroury, Oxidized G-C_3N_4/Polyaniline Nanofiber Composite for the Selective Removal of Hexavalent Chromium, *Sci. Rep.*, 2017, **7**(1), 12850, DOI: **10.1038/s41598-017-12850-1**.

57 K. Ding, X. Zhou, H. Hadiatullah, Y. Lu, G. Zhao, S. Jia, R. Zhang and Y. Yao, Removal Performance and Mechanisms of Toxic Hexavalent Chromium (Cr(VI)) with $ZnCl_2$ Enhanced Acidic Vinegar Residue Biochar, *J. Hazard. Mater.*, 2021, **420**, 126551, DOI: **10.1016/j.jhazmat.2021.126551**.

58 Q. Zhou, J. Huang, X. Zhang and Y. Gao, Assembling Polypyrrole Coated Sepiolite Fiber as Efficient Particle Adsorbent for Chromium(VI) Removal with the Feature of Convenient Recycling, *Appl. Clay Sci.*, 2018, **166**, 307–317, DOI: **10.1016/j.clay.2018.09.031**.

59 G. Chen, C. Qiao, Y. Wang and J. Yao, Synthesis of Magnetic Gelatin and Its Adsorption Property for Cr(VI), *Ind. Eng. Chem. Res.*, 2014, **53**(40), 15576–15581, DOI: **10.1021/ie502709u**.

60 L. A. Rodrigues, L. J. Maschio, R. E. Da Silva and M. L. C. P. Da Silva, Adsorption of Cr(VI) from Aqueous Solution by Hydrous Zirconium Oxide, *J. Hazard. Mater.*, 2010, **173**(1–3), 630–636, DOI: **10.1016/j.jhazmat.2009.08.131**.

61 A. Al Shra'ah, A. T. Al-Fawwaz, M. M. Ibrahim and E. Alsbou, Remediation of Methyl Orange Dye in Aqueous Solutions by Green Microalgae (Bracteacoccus Sp.): Optimization, Isotherm, Kinetic, and Thermodynamic Studies, *Separations*, 2024, **11**(6), 170, DOI: **10.3390/separations11060170**.

62 H. Zeng, H. Zeng, H. Zhang, A. Shahab, K. Zhang, Y. Lu, I. Nabi, F. Naseem and H. Ullah, Efficient Adsorption of Cr (VI) from Aqueous Environments by Phosphoric Acid Activated Eucalyptus Biochar, *J. Cleaner Prod.*, 2021, **286**, 124964, DOI: **10.1016/j.jclepro.2020.124964**.

63 A. Mohamed, L. Yu, Y. Fang, N. Ashry, Y. Riahi, I. Uddin, K. Dai and Q. Huang, Iron Mineral-Humic Acid Complex Enhanced Cr(VI) Reduction by Shewanella Oneidensis MR-1, *Chemosphere*, 2020, **247**, 125902, DOI: **10.1016/j.chemosphere.2020.125902**.

64 S. Banerjee, S. Dubey, R. K. Gautam, M. C. Chattopadhyaya and Y. C. Sharma, Adsorption Characteristics of Alumina Nanoparticles for the Removal of Hazardous Dye, Orange G from Aqueous Solutions, *Arab. J. Chem.*, 2019, **12**(8), 5339–5354, DOI: **10.1016/j.arabjc.2016.12.016**.

65 Y. Gu, X. Chen, L. Liu, S. Wang, X. Yu, Z. Jia and X. Zhou, Cr (VI)-Bioremediation Mechanism of a Novel Strain Bacillus Paramycoides Cr6 with the Powerful Ability to Remove Cr(VI) from Contaminated Water, *J. Hazard. Mater.*, 2023, **455**, 131519.

66 B. Eyvazi, A. Jamshidi-Zanjani and A. K. Darban, Synthesis of Nano-Magnetic $MnFe_2O_4$ to Remove Cr(III) and Cr(VI) from Aqueous Solution: A Comprehensive Study, *Environ. Pollut.*, 2020, **265**, 113685.

67 M. Elhoudi, A. Hsini, M. El Houdi, R. Lakhmiri and A. Albourine, A Theoretical Investigation of Complexation for Pyrimidine Bases with Hg^{2+} and Cd^{2+} by DFT Method, *Nanotechnol. Environ. Eng.*, 2021, **6**(2), 1–13, DOI: **10.1007/s41204-021-00128-x**.

68 T. Laktif, A. Imgharn, A. Hsini, M. Elhoudi, N. Aarab, M. Laabd, R. Lakhmiri and A. Albourine, Sunflower Seed Shells@ Polyaniline: A Novel Composite for the Removal of Pharmaceutical Pollutants from Wastewater, *Int. J. Environ. Anal. Chem.*, 2022, 1–18.

69 V. Choudhary, A. Bhatt, D. Dash and N. Sharma, DFT Calculations on Molecular Structures, HOMO–LUMO Study, Reactivity Descriptors and Spectral Analyses of Newly Synthesized Diorganotin(IV) 2-chloridophenylacetohydroxamate Complexes, *J. Comput. Chem.*, 2019, **40**(27), 2354–2363.

70 D. B. Boyd, The Power of Computational Chemistry to Leverage Stress Testing of Pharmaceuticals, *In Pharmaceutical stress testing*, CRC Press, 2005, pp 377–440.

71 J. Aires-de-sousa, Machine Learning Methods to Predict Density Functional Theory B3LYP Energies of HOMO and LUMO Orbitals, *J. Chem. Inf. Model.*, 2017, **57**(1), 11–21, DOI: **10.1021/acs.jcim.6b00340**.

72 M. Elhoudi, R. Oukhrib, C. A Celaya, D. G. Araiza, Y. Abdellaoui, I. Barra, Y. Brahmi, H. Bourzi, M. Reina, A. Albourine and H. Abou Oualid, Comparison of Green Bio-Based Cerium/Alginate *vs.* Copper/Alginate Beads: A Study of Vibrational and Thermal Properties Using

Experimental and Theoretical Methods, *J. Mol. Model.*, 2022, **28**(2), 1–15.

73 M. Miar, A. Shiroudi, K. Pourshamsian, A. R. Oliaey and F. Hatamjafari, Theoretical Investigations on the HOMO–LUMO Gap and Global Reactivity Descriptor Studies, Natural Bond Orbital, and Nucleus-Independent Chemical Shifts Analyses of 3-Phenylbenzo[d]Thiazole-2(3*H*)-Imine and Its Para-Substituted Derivatives: Solvent and Substituent Effects, *J. Chem. Res.*, 2021, **45**(1–2), 147–158.

74 P. Hobza, H. L. Selzle and E. W. Schlag, Potential Energy Surface of the Benzene Dimer: Ab Initio Theoretical Study, *J. Am. Chem. Soc.*, 1994, **116**(8), 3500–3506.

75 N. Malikova, I. Pastoriza-Santos, M. Schierhorn, N. A. Kotov and L. M. Liz-Marzán, Layer-by-Layer Assembled Mixed Spherical and Planar Gold Nanoparticles: Control of Interparticle Interactions, *Langmuir*, 2002, **18**(9), 3694–3697.

76 R. Haounati, H. Ighnih, R. E. Malekshah, S. Alahiane, F. Alakhras, E. Alabbad, H. Alghamdi, H. Ouachtak, A. A. Addi and A. Jada, Exploring ZnO/Montmorillonite Photocatalysts for the Removal of Hazardous RhB Dye: A Combined Study Using Molecular Dynamics Simulations and Experiments, *Mater. Today Commun.*, 2023, **35**, 105915.

77 I. Salahshoori, A. Mohseni, M. N. Jorabchi, S. Ghasemi, M. Afshar and S. Wohlrab, Study of Modified PVDF Membranes with High-Capacity Adsorption Features Using Quantum Mechanics, Monte Carlo, and Molecular Dynamics Simulations, *J. Mol. Liq.*, 2023, **375**, 121286.

78 I. Lebkiri, B. Abbou, R. Hsissou, Z. Safi, M. Sadiku, A. Berisha, A. El Amri, Y. Essaadaoui, L. Kadiri and A. Lebkiri, Investigation of the Anionic Polyacrylamide as a Potential Adsorbent of Crystal Violet Dye from Aqueous Solution: Equilibrium, Kinetic, Thermodynamic, DFT, MC and MD Approaches, *J. Mol. Liq.*, 2023, **372**, 121220.

79 P. Taylor; R. L. C. Akkermans; N. A. Spenley and S. H. Robertson, Monte Carlo Methods in Materials Studio, *Molecular Simulation*, Taylor & Francis, 2013, pp. 1153–1164, DOI: **10.1080/08927022.2013.843775**.

80 X. Xing, X. Ren, N. S. Alharbi and C. Chen, Efficient Adsorption and Reduction of Cr(VI) from Aqueous Solution by Santa Barbara Amorphous-15 (SBA-15) Supported Fe/Ni Bimetallic Nanoparticles, *J. Colloid Interface Sci.*, 2023, **629**, 744–754.

81 Y. Abdellaoui, C. A. Celaya, M. Elhoudi, R. Boualou, H. Agalit, M. Reina, P. Gamero-Melo and H. A. Oualid, Understanding of Vibrational and Thermal Behavior of Bio-Based Doped Alginate@nickel Cross-Linked Beads: A Combined Experimental and Theoretical Study, *J. Mol. Struct.*, 2022, **1249**, 131524, DOI: **10.1016/j.molstruc.2021.131524**.

82 K. Ait, E. Bacha, A. Imgharn, A. Hsini, H. Zouggari, F. Mahir, B. Selhami, R. Lakhmiri, M. Laabd, H. Ejazouli and A. Albourine, Arginine-Polyaniline Embedded Jujube Shells Composite for Outstanding Cr(VI) Detoxification from Aqueous Solution Arginine – Polyaniline Embedded Jujube Shells Composite for Outstanding Cr(VI) Detoxification from Aqueous Solution, *Water, Air, Soil Pollut.*, 2024, **235**, 380, DOI: **10.1007/s11270-024-07194-2**.

83 A. Hsini; R. Haounati; A. Imgharn; Y. Naciri; R. E. Malekshah; A. Shaim; S. Szunerits; R. Boukherroub and A. Albourine Carbon Nitride Nanostructures for Cr(VI) Adsorption in Water 2024, VI, DOI: **10.1021/acsanm.4c01503**.

84 Y. Abdellaoui, H. Abou, A. Hsini and B. El, Synthesis of Zirconium-Modified Merlinoite from Fly Ash for Enhanced Removal of Phosphate in Aqueous Medium: Experimental Studies Supported by Monte Carlo/SA Simulations, *Chem. Eng. J.*, 2021, **404**, 126600, DOI: **10.1016/j.cej.2020.126600**.